Low-temperature ferromagnetism in tensile-strained $LaCoO_{2.5}$ thin film

Yang-Yang Fan(范洋洋), Jing Wang(王晶), Feng-Xia Hu(胡凤霞), Bao-He Li(李宝河), Ai-Cong Geng(耿爱丛), Zhuo Yin(殷卓), Cheng Zhang(张丞), Hou-Bo Zhou(周厚博), Meng-Qin Wang(王梦琴), Zi-Bing Yu(尉紫冰), and Bao-Gen Shen(沈保根)

Citation: Chin. Phys. B, 2023, 32 (**8**): 087504. DOI: 10.1088/1674-1056/acafdc
Journal homepage: http://cpb.iphy.ac.cn; http://iopscience.iop.org/cpb

What follows is a list of articles you may be interested in

Crystal growth of $CeMn_{0.85}Sb_2$: Absence of magnetic order of Ce-sublattice

Yong Li(李勇), Shan-Shan Miao(苗杉杉), Hai Feng(冯海),Huai-Xin Yang(杨槐馨), and You-Guo Shi(石友国)
Chin. Phys. B, 2023, 32 (**6**): 067501. DOI: 10.1088/1674-1056/acc060

Prediction of $LiCrTe_2$ monolayer as a half-metallic ferromagnet with a high Curie temperature

Li-Man Xiao(肖丽蔓), Huan-Cheng Yang(杨焕成), and Zhong-Yi Lu(卢仲毅)
Chin. Phys. B, 2023, 32 (**5**): 057505. DOI: 10.1088/1674-1056/acbe2e

Perpendicular magnetic anisotropy of $Pd/Co_2MnSi/NiFe_2O_4/Pd$ multilayers on F-mica substrates

Qingwang Bai(白青旺), Bin Guo(郭斌), Qin Yin(尹钦), and Shuyun Wang(王书运)
Chin. Phys. B, 2022, 31 (**1**): 017501. DOI: 10.1088/1674-1056/ac20cc

Room temperature ferromagnetism in un-doped amorphous HfO_2 nano-helix arrays

Xie Qian (谢谦), Wang Wei-Peng (王炜鹏), Xie Zheng (谢拯), Zhan Peng (战鹏), Li Zheng-Cao (李正操), Zhang Zheng-Jun (张政军)
Chin. Phys. B, 2015, 24 (**5**): 057503. DOI: 10.1088/1674-1056/24/5/057503

Defect types and room temperature ferromagnetism in N-doped rutile TiO_2 single crystals

Qin Xiu-Bo (秦秀波), Li Dong-Xiang (李东翔), Li Rui-Qin (李瑞琴), Zhang Peng (张鹏), Li Yu-Xiao (李玉晓), Wang Bao-Yi (王宝义)
Chin. Phys. B, 2014, 23 (**6**): 067502. DOI: 10.1088/1674-1056/23/6/067502

Low-temperature ferromagnetism in tensile-strained $LaCoO_{2.5}$ thin film

Yang-Yang Fan(范洋洋)[1,2], Jing Wang(王晶)[1,3,†], Feng-Xia Hu(胡凤霞)[1,3,4,‡], Bao-He Li(李宝河)[2,§], Ai-Cong Geng(耿爱丛)[2], Zhuo Yin(殷卓)[1,3], Cheng Zhang(张丞)[1,3], Hou-Bo Zhou(周厚博)[1,3], Meng-Qin Wang(王梦琴)[1,3], Zi-Bing Yu(尉紫冰)[1,3], and Bao-Gen Shen(沈保根)[1,3,4,5]

[1] *Beijing National Laboratory for Condensed Matter Physics and State Key Laboratory of Magnetism, Institute of Physics, Chinese Academy of Sciences, Beijing* 100190, *China*

[2] *School of Physics, Beijing Technology and Business University, Beijing* 100048, *China*

[3] *School of Physical Sciences, University of Chinese Academy of Sciences, Beijing* 101408, *China*

[4] *Songshan Lake Materials Laboratory, Dongguan* 523808, *China*

[5] *Ningbo Institute of Materials Technology and Engineering, Chinese Academy of Sciences, Ningbo* 315201, *China*

(Received 16 September 2022; revised manuscript received 11 November 2022; accepted manuscript online 4 January 2023)

The origin of ferromagnetism in epitaxial strained $LaCoO_{3-x}$ films has long been controversial. Here, we investigated the magnetic behavior of a series of oxygen vacancy-ordered $LaCoO_{3-x}$ films on different substrates. Obvious ferromagnetism was observed in perovskite $LaCoO_3$/LSAT (LSAT = $(LaAlO_3)_{0.3}(SrAlTaO_6)_{0.7}$) and $LaCoO_3/SrTiO_3$ films, while $LaCoO_3/LaAlO_3$ films showed weak ferromagnetic behavior. Meanwhile, $LaCoO_{2.67}$ films exhibited antiferromagnetic behavior. An unexpected low-temperature ferromagnetic phenomenon with a Curie temperature of $\sim$ 83 K and a saturation magnetization of $\sim$ 1.2 μ_B/Co was discovered in 15 nm thick $LaCoO_{2.5}$/LSAT thin films, which is probably related to the change in the interface CoO_6 octahedron rotation pattern. Meanwhile, the observed ferromagnetism gradually disappeared as the thickness of the film increased, indicating a relaxation of tensile strain. Analysis suggests that the rotation and rhombohedral distortion of the CoO_6 octahedron weakened the crystal field splitting and promoted the generation of the ordered high-spin state of Co^{2+}. Thus the super-exchange effect between Co^{2+} (high spin state), Co^{2+} (low spin state) and Co^{2+}(high spin state) produced a low-temperature ferromagnetic behavior. However, compressive-strained $LaCoO_{2.5}$ film on a $LaAlO_3$ substrate showed normal anti-ferromagnetic behavior. These results demonstrate that both oxygen vacancies and tensile strain are correlated with the emergent magnetic properties in epitaxial $LaCoO_{3-x}$ films and provide a new perspective to regulate the magnetic properties of transition oxide thin films.

Keywords: transition metal oxides films, oxygen vacancy, topological phase transitions, magnetism

PACS: 75.70.–I, 75.30.kz, 75.47.Lx, 72.15.–v **DOI:** 10.1088/1674-1056/acafdc

1. Introduction

Transition metal oxides (TMOs) are characterized by strong correlations that exhibit rich physical phenomena, including semiconductivity, superconductivity, charge-ordering and spin-ordering, ferromagnetism, giant magnetoresistance and other properties. TMOs also exhibit the flexibility of chemical doping as well as potentially useful physicochemical properties, and are thus extremely valuable for basic research and commercial applications. Interestingly, the useful properties of TMOs can often be achieved through delicate structural tuning via strain engineering, dimensionality and superlattice ordering. Two well known examples of TMOs are magnetism and cuprate, the former exhibits colossal magnetoresistance (CMR), and the latter is a high-temperature superconductor.[1–5] In addition, defects in crystal structures can also effectively regulate the properties of materials. For example, oxygen vacancies (Vo) are one of the most common point defects that play a key role in regulating the physicochemical properties of oxides due to their unique chemical, physical and ionic properties. Precise epitaxial growth of perovskite structural oxide films has been achieved experimentally, making it possible to study the phenomenon of heterogeneous interface evolution of strongly correlated electronic systems.[6–8] Exploring the origin of these extraordinary phenomena in TMOs is challenging.

Lanthanum cobaltite ($LaCoO_3$) epitaxial film is a typical example of a TMO. It is generally known that bulk $LaCoO_3$ is diamagnetic with Co ions in the low spin state (LS, $t_{2g}^6e_g$, $S = 0$) at low temperatures; however, this changes to an intermediate-spin state (IS, $t_{2g}^5e_g^1$, $S = 1$) or high-spin state (HS, $t_{2g}^4e_g^2$, $S = 2$) with increasing temperature.[9] Previous work creatively discovered low-temperature ferromagnetism (FM) in epitaxial $LaCoO_3$ films with in-plane tensile strain. Thereafter, the origin of this behavior has attracted much attention and many experiments and theoretical studies have been carried out.[10,11] Various physical mechanisms

†Corresponding author. E-mail: wangjing@.iphy.ac.cn

‡Corresponding author. E-mail: fxhu@.iphy.ac.cn

§Corresponding author. E-mail: lbhe@th.btbu.edu.cn

have been put forward to explain the origin of magnetization in $LaCoO_3$ films. Recently, it has been documented that tensile strain reduces the bond angle of Co–O (β) and increases the length of the Co–O–Co bond (d). This is conducive to increasing the bandwidth of the energy band and reducing the crystal field splitting effect (Δ_{CF}), hence showing an advantage in occupation of IS/HS states and leading to low-temperature ferromagnetism.[12,13] HS and IS states and the combination of disordered and ordered phases have been deduced in tensile-strained $LaCoO_3$ films, from x-ray absorption near-edge spectroscopy, x-ray magnetic circular dichroism, x-ray magnetic linear dichroism and scanning transmission electron microscopy electron energy loss spectroscopy. It has also been demonstrated that the tuning of epitaxial strain causes a direct change in the magnetic properties.[14,15] However, epitaxial strain does not fully explain the novel physical phenomena in $LaCoO_3$ films. In the past several years, researchers have found that the Vo concentration is also important in high-temperature superconductors, metal−insulator transition, CMR, ferroelectric polarity, etc.[16,17] Hence, the role of Vo in $LaCoO_{3-x}$ films must also be taken into consideration. It has been reported that Vo cause the lattice to expand, which could directly weaken the epitaxial strain of the film. Meanwhile, reduction in the content of HS Co^{3+} ions and direct inhibition of the ferromagnetic super-exchange of the film[18] results in an antiferromagnetic ground state due to the increasing content of Vo with the increase in Co^{2+} (LS). Previous work indicates that V_O-ordered $LaCoO_{2.67}$ and brownmillerite $LaCoO_{2.5}$ (BM-LCO) films show strong antiferromagnetic behavior, which is ascribed to the transition in the spin state of Co ions accompanying the appearance of V_O-ordered channels.[19] On the contrary, some recent works suggest that ordered Vo probably also lead to the generation of long-range ferromagnetic order via the HS Co^{2+} cations.[20] To date, the origin of ferromagnetism in $LaCoO_{3-x}$ films is still controversial, and it is very challenging to explore the key elements of ferromagnetism in $LaCoO_{3-x}$ thin films.

Here, we have investigated systematically the combined effects of ordered Vo and epitaxial strain on magnetism in epitaxial $LaCoO_{3-x}$ thin films. Through a comparative study of epitaxial $LaCoO_{3-x}$ films using a superconducting quantum interference device–vibrating sample magnetometer (SQUID-VSM) with perovskite $LaCoO_3$ (PV-LCO), BM-LCO and $LaCoO_{2.67}$ phases, which were grown on $LaAlO_3$ (LAO), $(LaAlO_3)_{0.3}(SrAlTaO_6)_{0.7}$ (LSAT), and $SrTiO_3$ (STO) substrates, respectively, we found unexpectedly that 15 nm thick BM-LCO film exhibits low-temperature ferromagnetism with a Curie temperature (T_c) of $\sim$ 83 K and saturation magnetization of $\sim$ 1.2 μ_B/Co. Moreover, the observed low-temperature ferromagnetism gradually disappears as the thickness of the film increases and analysis suggests that this may originate from the interface effect.[21] We believe that this novel phenomenon may be caused by the rotation and rhombohedral distortion of the CoO_6 octahedron and the ordered Vo due to tensile strain.[22,23] In contrast, the compressively strained BM-LCO film on LAO exhibits anti-ferromagnetic behavior. The reason for this physical phenomenon should be those extra electrons induced by Vo and causing a transition from HS Co^{3+} to LS Co^{2+}, which contains half-occupied e_g orbitals supporting anti-ferromagnetic super-exchange.[24–26] The results provide a new aspect for understanding the origin of ferromagnetism in strained epitaxial $LaCoO_{3-x}$ films.

2. Experimental details

High-quality PV-LCO films were epitaxially grown on a series of single-crystalline substrates by pulsed-laser deposition, including LAO, LSAT and STO. The room-temperature in-plane lattice parameters a_{sub} of the substrates and the corresponding lattice mismatch to $LaCoO_{3-x}$, $\varepsilon = (a_{sub} - a_{LCO})/a_{sub} \times 100\%$, where a_{LCO} corresponds to the lattice parameters of the bulk $LaCoO_3$ and pseudocubic $LaCoO_{2.5}$. The lattice mismatch ranges from $\varepsilon = -0.74\%$ for $LaCoO_3$ films on LAO to $\varepsilon = +2.17\%$ for films on STO and from $\varepsilon = -1.50\%$ for $LaCoO_{2.5}$ films on LAO to $\varepsilon = +0.49\%$ for films on LSAT (Fig. 1). A KrF laser ($\lambda = 248$ nm) with a frequency of 2 Hz was used to ablate the stoichiometric target. The $LaCoO_3$ target was prepared by the conventional solid reaction method. During the deposition, the temperature of the substrate was kept at 700 °C and the oxygen pressure at 30 Pa. This results in deposition rates of around 13 Å·min^{-1}. After deposition, the films were annealed in a pure oxygen atmosphere of 100 Pa at 700 °C for about 20 min to achieve full oxygenation of the samples. Samples were then cooled to room temperature at a rate of 5 °C·min^{-1} at an oxygen pressure of 100 Pa. The $LaCoO_{2.67}$ and BM-LCO samples were formed by post-annealing in a vacuum ($P \sim 10^{-6}$ Pa). The surface morphology analysis of the grown PV-LCO films was investigated by atomic force microscopy (AFM). The crystalline structure of thin films was characterized by x-ray diffraction (XRD) using Cu $K\alpha$ radiation on a Bruker AXS D8-Discover. X-ray reflectivity (XRR) measurements were conducted to determine the thickness and density of the films. Reciprocal space maps (RSMs) around substrate (–103) peaks indicate a strain relaxation (lattice constant) of 15–80 nm for BM-LCO films. A SQUID magnetometer was used to derive the total magnetization. The field-cooled (FC) magnetization was measured in the temperature range 10 K $\leq T \leq$ 300 K with an external magnetic field of $H = 500$ Oe applied parallel to the film surface.

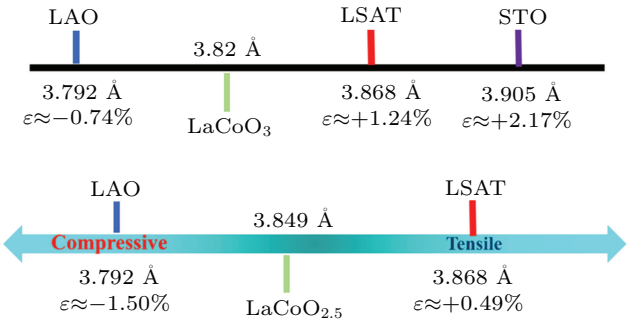

Fig. 1. Lattice mismatch between bulk $LaCoO_3$, pseudocubic $LaCoO_{2.5}$ and various substrates.

3. Results and discussion

XRR measurements were performed to verify the thickness of $LaCoO_3$; the results indicate that the films have uniform chemical distributions and are highly crystalline (Figs. 2(a)–2(c)). The insets show the x-ray scattering length density (SLD), which is proportional to the chemical density. To further survey the structural quality of the PV-LCO thin films under different substrates, AFM was used to perform a surface morphology analysis of the PV-LCO films (Figs. 2(d)–2(f)). The averaged RMS surface roughness is ∼ 0.3 nm, revealing a good epitaxial quality of the film and a smooth surface. Combined with the rocking curve of each $LaCoO_3$ (002) reflection with a single peak, shown in Figs. 3(g)–3(i), good *c*-axis orientation can be further affirmed. To evaluate the crystallization quality of the films, the full width at half maximum (FWHM) of $LaCoO_3$ (002) diffraction peaks was obtained; the structural FWHMs are 0.048° (LSAT), 0.17° (LAO) and 0.048° (STO). Figures 3(a)–3(c) show the XRD θ–2θ scan pattern of all films on LAO, LSAT and STO substrates, respectively; these indicate that the film was epitaxially grown on the substrate, with no other textures or phases being observed. Distinct thickness fringes around the Bragg peaks demonstrate the high quality of all $LaCoO_3$ films. Moreover, the out-of-plane (OOP) lattice constant *c* of PV-LCO films grown on LAO substrates (Fig. 3(a)) is determined to be ∼ 3.85 Å, while films on LSAT (Fig. 3(b)) and STO (Fig. 3(c)) have OOP lattice constants of ∼ 3.80 Å and ∼ 3.78 Å, respectively. This result also confirms that the perovskite film is under compressive strain on the LAO substrate while it is under tensile strain on the LSAT and STO substrates. Intriguingly, the OOP peaks for thick films on LSAT substrate show a significant shift in 2θ, suggesting that the lattice strain of the film gradually relaxes with increasing thickness.[27]

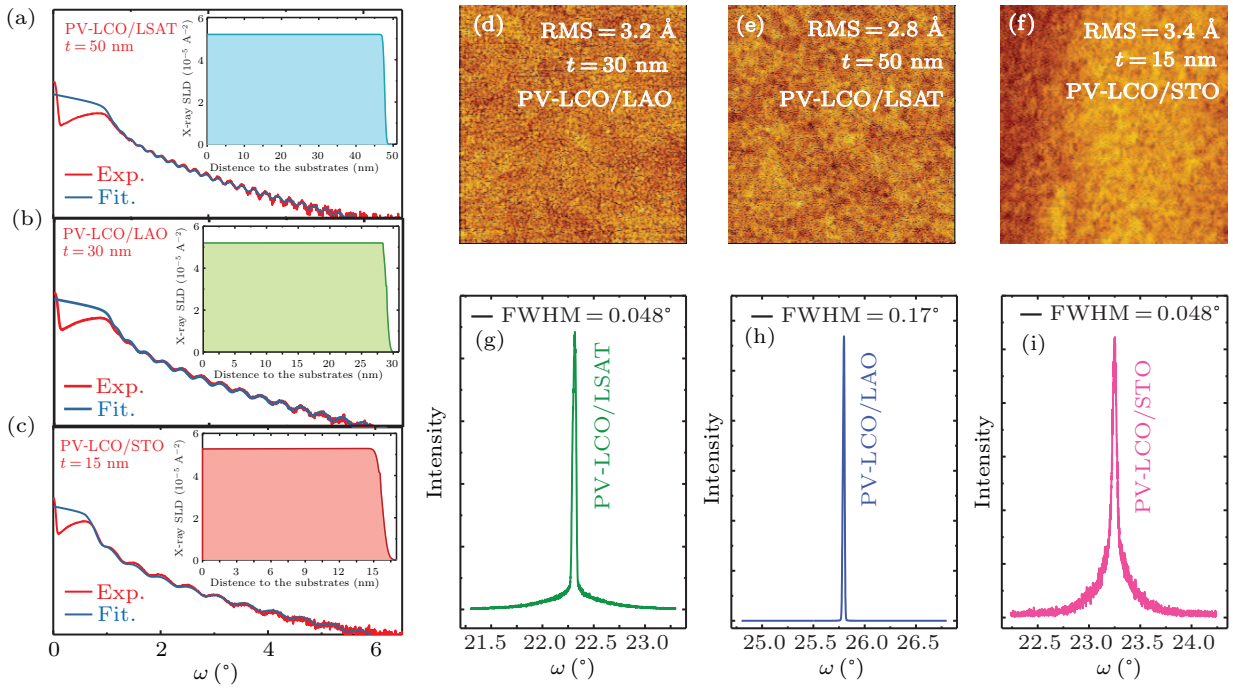

Fig. 2. Structure and morphological characterizations in $LaCoO_3$ thin films. The small-angle x-ray reflection and fitting curves of $LaCoO_3$ films on the (a) LSAT substrate, (b) LAO substrate and (c) STO substrate. The insets show the x-ray scattering length density. AFM images of $LaCoO_3$ films grown on (d) LAO substrate, (e) LSAT substrate and (f) STO substrate. The respective rocking curves of the $LaCoO_3$ (002) peaks on (g) LSAT substrate, (h) LAO substrate and (i) STO substrate.

The temperature (*T*)–magnetization (*M*)–magnetic field (*H*) of pristine PV-LCO samples is shown in Figs. 3(d)–3(f). The PV-LCO films on LSAT and STO substrates both exhibit clear evidence of low-temperature ferromagnetism, and the T_c values are all below 81 K. However, it is interesting that 15 nm thick PV-LCO film on LSAT substrate, which is under smaller tensile strain than the PV-LCO/STO film, has the highest saturation magnetization of ∼ 1.4 μ_B/Co (Fig. 3(e)). We found a lower saturated moment of ∼ 0.8 μ_B/Co (Fig. 3(f)) with tetragonal distortion.[28] Besides, Figs. 3(e) and 3(f) show that the

saturation moment on LSAT and STO decreases as a function of increasing thickness. These results indicate that PV-LCO films under tensile strain exhibit low-temperature ferromagnetic behavior. The tensile strain reduces the bond angle Co–O (β) and increases the length of the Co–O–Co bond (d), which is conducive to increasing the bandwidth of the energy band (e_g) and reducing the crystal field splitting effect (Δ_{CF}), hence showing an advantage in occupying the IS state and the HS state.[29] The reduction in FM response in thick films on LSAT and STO is expected due to structural relaxation. On the other hand, 15 nm PV-LCO film strained on LAO exhibits hardly any ferromagnetism, thus suggesting that compressive strain does not give rise to ferromagnetism. In contrast to 15 nm PV-LCO films, 50 nm PV-LCO film on LAO shows slightly ferromagnetic behavior. In these thicker films, the ferromagnetic behavior is obvious because the tetragonal distortion is much smaller.[30]

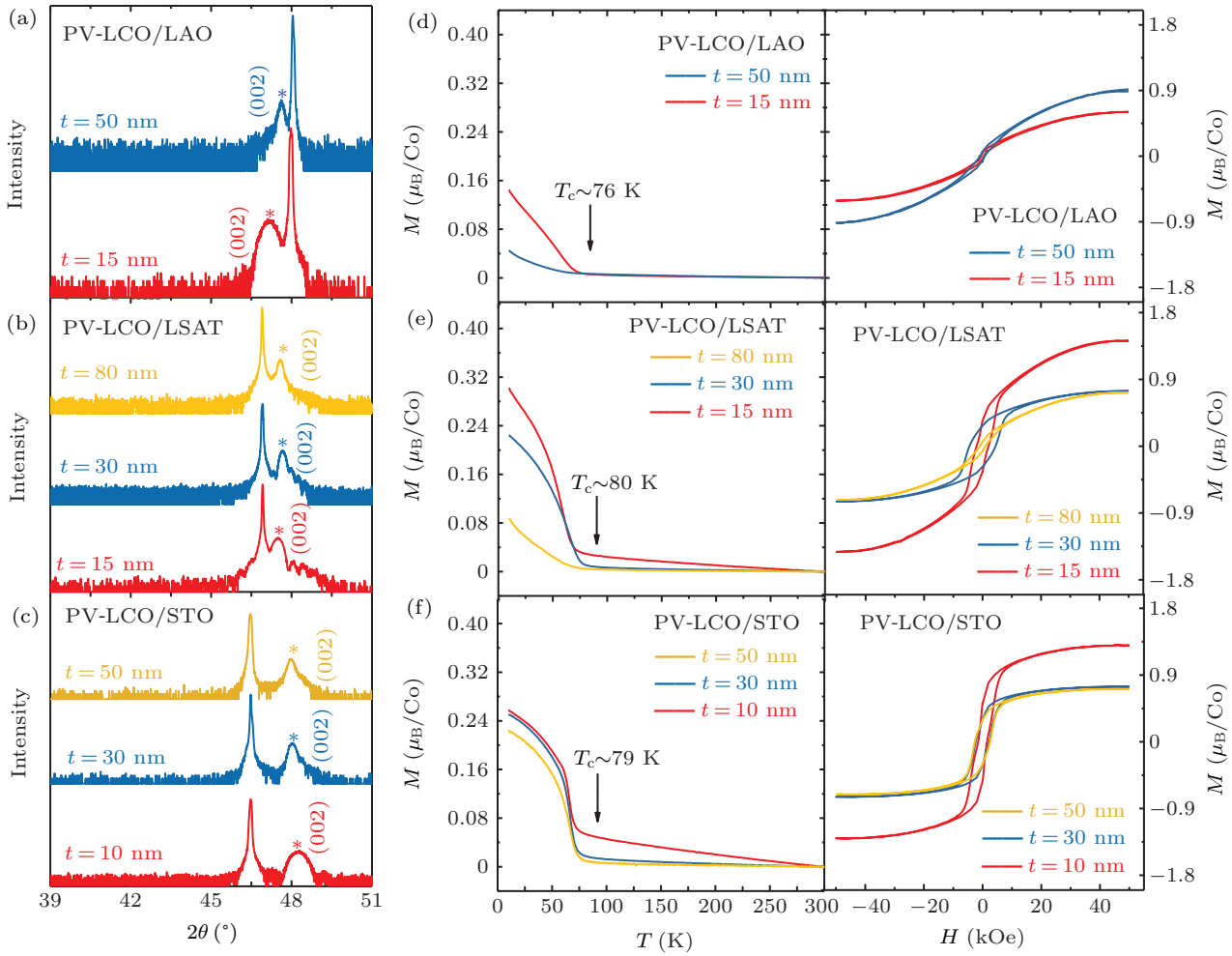

Fig. 3. XRD spectra (002) peaks of PV-LCO films on (a) LAO, (b) STO and (c) LSAT substrates. Magnetic properties of the PV-LCO phase films on (d) LAO, (e) STO and (f) LSAT substrates. M–T curves were measured by applying an in-plane magnetic field $\mu_0 H = 500$ Oe. Arrows indicate the Curie temperature of each film, as determined by the extrema of $\mathrm{d}M/\mathrm{d}T$. Magnetic hysteresis loops were measured at $T = 10$ K for PV-LCO thin films on different substrates.

Meanwhile, Vo also play a significant role in determining the properties of $LaCoO_{3-x}$ films. There have been successful examples in which the properties of $LaCoO_{3-x}$ films were designed by tuning the concentration of Vo. The earlier works show that the crystal structure of BM-LCO is a pseudocubic crystal system ($a = 3.849$ Å). The BM-LCO films show no ferromagnetic behavior of the hysteresis loop. A transition from Co^{3+} (HS) to Co^{2+} (LS) is implemented by extra electrons introduced by Vo, and an antiferromagnetic ground state is easier to form with Co^{2+} (LS).[31–35] However, our work found low-temperature ferromagnetism in 15 nm thick BM-LCO film on LSAT. In addition, the saturation magnetization ($\sim 1.2\ \mu_B$/Co) is larger than that of 50 nm thick PV-LCO film on LSAT. Here, the PV-LCO films on LSAT substrates of different thicknesses were annealed at 450 °C for 4 h and 500 °C for 4 h, which accomplished the topological phase transition from the PV-LCO phase into $LaCoO_{2.67}$ and the BM-LCO phase (Figs. 4(a)–4(c)). The BM-LCO films can be inferred from the XRD spectra. A series of peaks at about 33.7°, 45.4° and 57.7°, corresponding to the (006), (008) and (0010) diffractions, are observed. These are ascribed to the alternate octahedral and tetrahedral layers in the brownmillerite

structure. The $LaCoO_{2.67}$ phase films can be inferred from the XRD spectra. A series of peaks at about 15.2°, 30.3°, 38.4° and 54.4°, corresponding to the (002/3), (004/3), (005/3) and (007/3) diffractions, are observed. To better understand the overall structural changes as a function of the LSAT substrate, we compared RSMs for 15–80 nm thick films and found different degrees of relaxation of the films (Fig. 5(a)).

The magnetic properties were examined in $LaCoO_{2.5}$ films grown on LSAT substrates. Interestingly, ferromagnetism is found in 15 nm thick BM-LCO film on LSAT, which exhibits a magnetic phase transition at $T_c \sim 83$ K and clear hysteresis loops where the coercive force is about 700 Oe. The peculiar rotation and rhombohedral distortion of the CoO_6 octahedron may be induced by tensile strain. Hence, the electron arrangement of the e_g and t_{2g} orbitals is changed, reducing the crystal field splitting energy Δ_{CF} and producing a HS state ($t_{2g}^4 e_g^2$, $S = 2$).[36] Moreover, rhombohedral distortion and rotation of the CoO_6 octahedron are easier to maintain in the $LaCoO_{2.5}$/LSAT interface, and Jahn–Teller distortion of the CoO_4 tetragonal is inhibited by hybridization between the 3d orbital of Co and the 2p orbital of O.[37] Therefore, a possible explanation for the ferromagnetic behavior in 15 nm thick BM-LCO film is the presence of a super-exchange effect between Co^{2+} (HS), Co^{2+} (LS) and Co^{2+} (HS). Meanwhile, we found that the 80 nm BM-LCO or $LaCoO_{2.67}$ film on LSAT does not show low-temperature ferromagnetism. As the thickness increases, the strain of the film will gradually relax, which is not conducive to the existence of Co^{2+} (HS).[38] RSM confirms this speculation (Fig. 5(a)). Meanwhile, a comparison of the optical diagram of the topological phase is shown in Fig. 5(b), and the three phases exhibit a noticeable color difference. The greater the concentration of Vo in the film, the lighter the color of the film, which further proves that the band gap of the BM-LCO film is maximal.

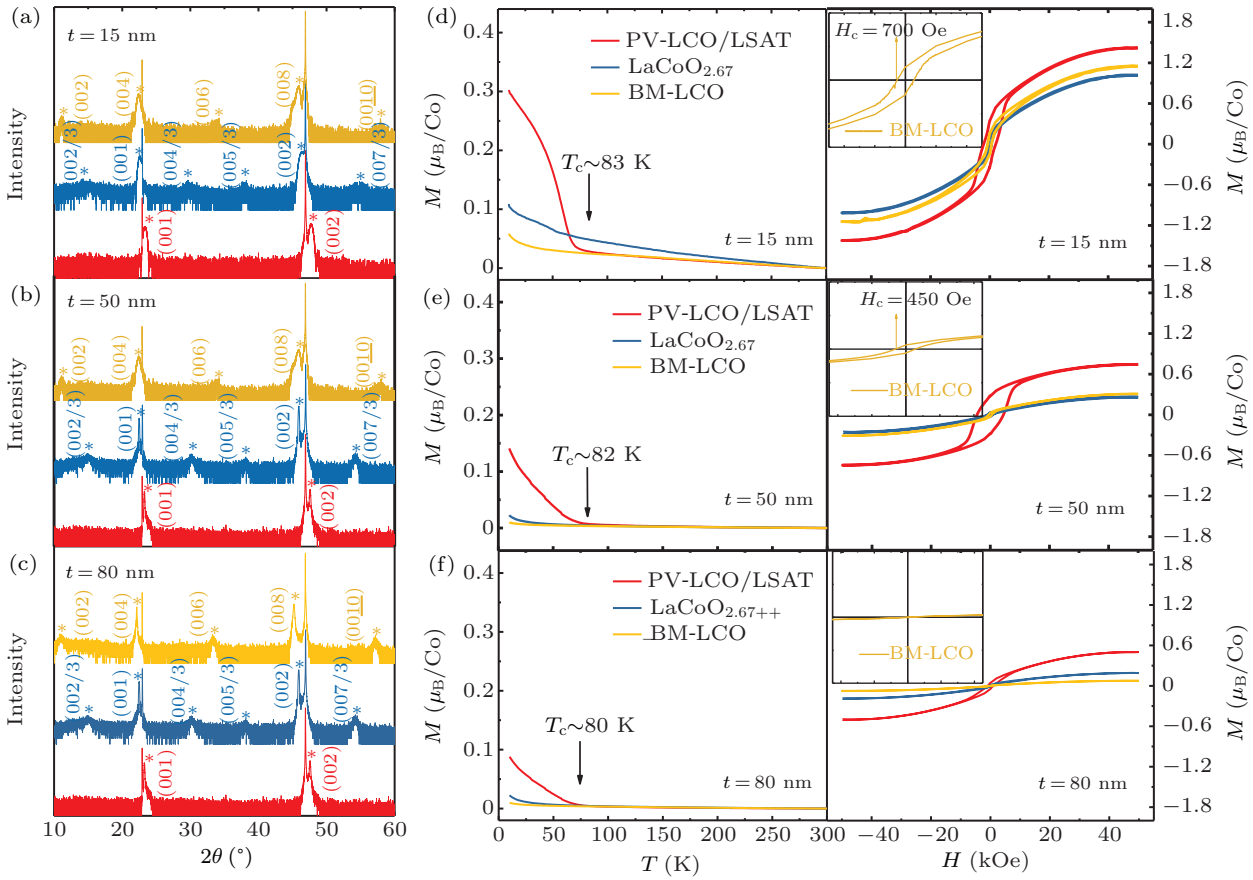

Fig. 4. (a)–(c) XRD θ–2θ scans, (d)–(f) M–T and M–H curves of PV-LCO/LSAT (red), BM-LCO/LSAT (orange) and $LaCoO_{2.67}$/LSAT (blue) films. The inset in the right panels (d)–(f) The local isothermal magnetization curves (M–H) of different BM-LCO thin films at 10 K.

To better compare the influence of compressive and tensile strain on the magnetism of the film, $LaCoO_{2.67}$ and BM-LCO films on LAO were also formed by annealing the PV-LCO/LAO film in a vacuum ($P \sim 10^{-6}$ Pa) at 450 °C for 4 h and 500 °C for 2 h, respectively. Figure 6(a) shows the XRD patterns of $LaCoO_{3-x}$ film (50 nm thick) on LAO. The BM-LCO films can be inferred from the XRD. A series of peaks at about 33.7°, 45.4° and 57.7°, corresponding to the (006), (008) and (0010) reflections, are observed, which can be ascribed to the alternate octahedral and tetrahedral layers in the brownmillerite structure. The $LaCoO_{2.67}$ phase films can be inferred from the XRD spectra. A series of peaks at 15.2°, 30.3°, 38.4° and 54.4°, corresponding to the (002/3), (004/3), (005/3) and (007/3) reflections, are observed (Fig. 6(a)).

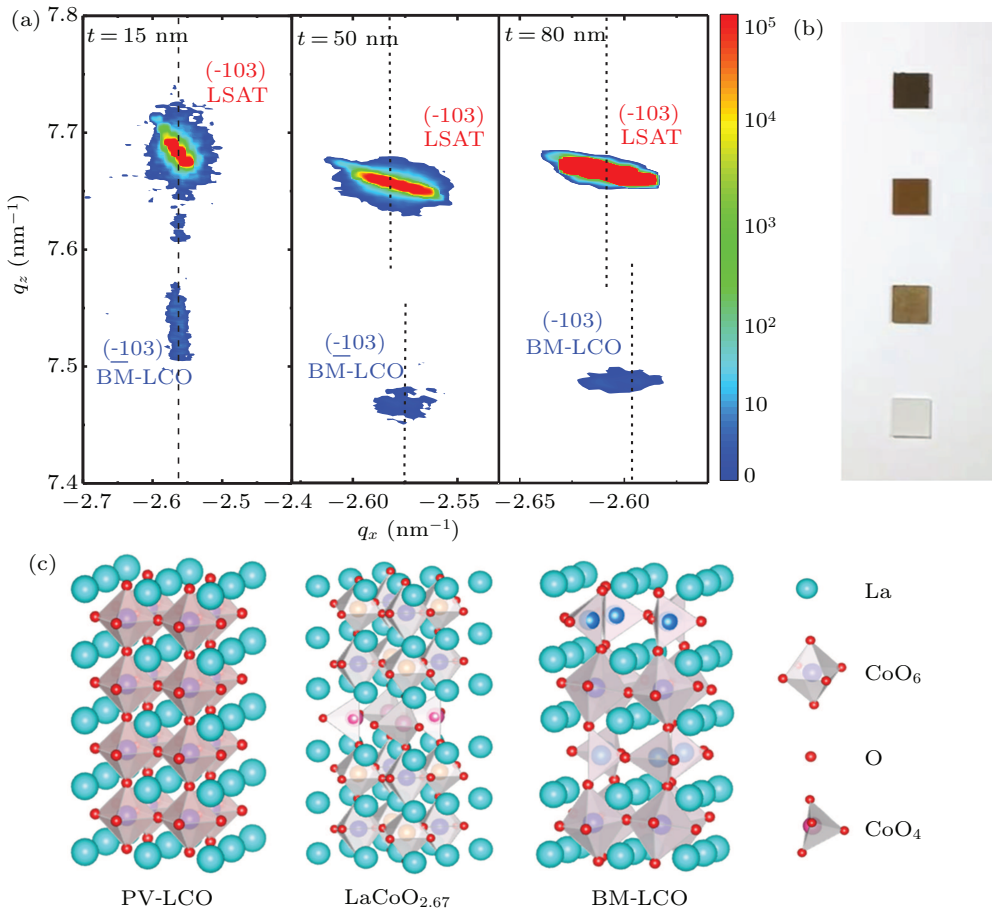

Fig. 5. (a) Reciprocal space maps of (–103) peak reflections for the 15 nm, 50 nm and 80 nm BM-LCO films grown on LSAT. (b) Comparison of the optical diagram of the topological phases. (c) Crystal structures of PV-LCO, $LaCoO_{2.67}$ and BM-LCO phases.

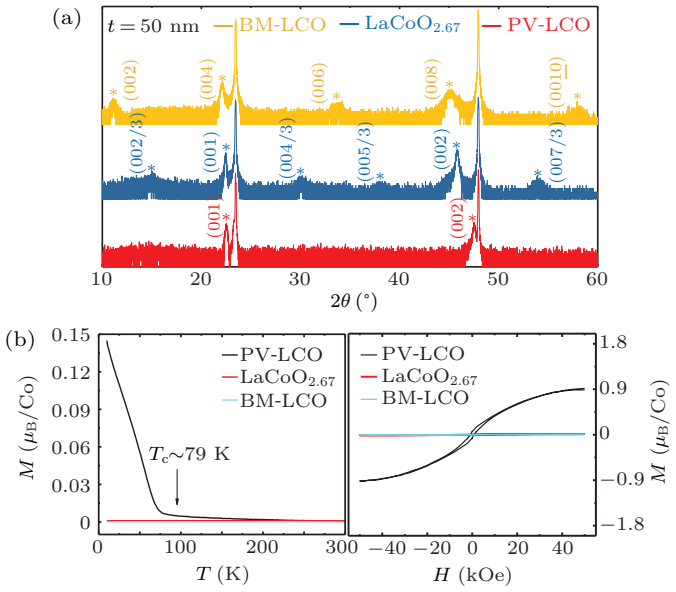

Fig. 6. Structural evolution and magnetic properties of $LaCoO_{3-x}$ films. (a) XRD θ–2θ scan of PV-LCO, $LaCoO_{2.67}$ and BM-LCO films grown on LAO. (b) M–T and M–H curves of PV-LCO, $LaCoO_{2.67}$ and BM-LCO films.

The magnetic properties of 50 nm thick films grown on LAO substrate are shown in Fig. 6(b). The ferromagnetism of BM-LCO and $LaCoO_{2.67}$ film disappears completely and antiferromagnetic behavior appears. This result is consistent with previous reports from first-principles calculations, which demonstrated that the cohesive energy of the Co–O bond in CoO_4 tetrahedra is more unstable than that in CoO_6 octahedra. In addition, a transition from Co^{3+} (HS) to Co^{2+} (LS) occurs due to Vo-induced extra electrons, while the latter, containing half-occupied e_g orbitals, favor antiferromagnetic superexchange. The magnetic behavior matches well with the result for the reported G-type antiferromagnetic in BM-LCO.[39,40]

4. Conclusions

In conclusion, we investigated the magnetic behavior of a collection of Vo-ordered $LaCoO_{3-x}$ films. Pronounced ferromagnetism was observed in perovskite $LaCoO_3$/LSAT and $LaCoO_3$/STO films, but weak ferromagnetism in $LaCoO_3$/LAO films. Meanwhile, $LaCoO_{2.67}$ films exhibit antiferromagnetic behavior. More interestingly, an unexpected low-temperature ferromagnetic state was found in 15 nm thick BM-LCO/LSAT film that gradually disappears with increasing film thickness. However, no ferromagnetic behavior was observed in BM-LCO film on LAO substrate. Our result casts into doubt the present hypothesis that BM-LCO is always anti-ferromagnetic. Considering that the tensile strain in our LCO/LSAT film can induce peculiar CoO_6 rotation and rhombohedral distortion, which results in the ordered high-

spin state of Co^{2+} and weakens the crystal field splitting energy (Δ_{CF}), the observed low-temperature ferromagnetic behavior in 15 nm thick BM-LCO film may be due to the presence of a super-exchange effect between Co^{2+} (HS), Co^{2+} (LS) and Co^{2+} (HS). These results suggest that tensile strain could be considered vital for the magnetometry of $LaCoO_{3-x}$ films, which puts forward a new idea for understanding the origin of the magnetism of $LaCoO_{3-x}$ film. This would have very good application value in the fields of ion conductors and electrochemical sensors.

Acknowledgements

This work was supported by the National Key Research and Development Program of China (Grant Nos. 2020YFA0711502 and 2019YFA0704900), the National Natural Sciences Foundation of China (Grant Nos. 52088101, 51971240, and 11921004), the Key Program of the Chinese Academy of Sciences and the Strategic Priority Research Program (B) of the Chinese Academy of Sciences (Grant No. XDB33030200).

References

[1] Ngai J H, Walker F J and Ahn C H 2014 *Annu Rev. Mater. Res.* **44** 1
[2] Ling Z B, Zhang Q Y, Yang C P, Li X T, Liang W S, Wang Y Q, Yang H W and Sun J R 2020 *Chin. Phys. B* **29** 096802
[3] Jeong J, Aetukuri N, Graf T, Schladt T, Samant M and Parkin S 2013 *Science* **339** 1402
[4] Imada M, Fujimori A and Tokura Y 1998 *Rev. Mod. Phys.* **70** 1039
[5] Guo E J, Desautels R, Keavney D, Roldan M A, Kirby B J, Lee D, Liao Z L, Charlton T, Herklotz A, Ward T Z, Fitzsimmons M R and Lee H N 2019 *Sci. Adv.* **5** evav5050
[6] Fuchs D, Pinta C, Schwarz T, Schweiss P, Nagel P, Schuppler S, Schneider R, Merz M, Roth G and Löhneysen H V 2007 *Phys. Rev. B* **75** 144402
[7] Fuchs D, Arac E, Pinta C, Schuppler S, Schneider R and Löhneysen H V 2008 *Phys. Rev. B* **77** 014434
[8] Jeen H, Choi W S, Freeland J W, Ohta H, Jung C U and Lee H N 2013 *Adv. Mater.* **25** 3651
[9] Fujioka J, Yamasaki Y, Nakao H, Kumai R, Murakami Y, Nakamura M, Kawasaki M and Tokura Y 2013 *Phys. Rev. Lett.* **111** 027206
[10] Chaturvedi V, Walter J, Paul A, Grutter A, Kirby B, Jeong J S, Zhou H, Zhang Z, Yu B Q, Greven M, Mkhoyan K A, Birol T and Leighton C 2020 *Phys. Rev. Mater.* **4** 034403
[11] G J la O', Ahn S J, Crumlin E, Orikasa Y, Biegalski M D, Christen H M and Yang S H 2010 *Angew. Chem. Int. Ed.* **49** 5344
[12] Phelan D, Louca D, Kamazawa K, Lee S H, Ancona S N, Rosenkranz S, Motome Y, Hundley M F, Mitchell J F and Moritomo Y 2006 *Phys. Rev. Lett.* **97** 235501
[13] Becher C, Maurel L, Aschauer U, Lilienblum M, Magén C, Meier D, Langenberg E, Trassin M, Blasco J, Krug I P, Algarabel P A, Spaldin N A, Pardo J A and Fiebig M 2015 *Nat. Nanotechnol.* **10** 661
[14] Kalinin S V and Spaldin N A 2013 *Science* **341** 858
[15] Mehta V V, Biskup N, Jenkins C, Arenholz E, Varela M and Suzuki Y 2015 *Phys. Rev. B* **91** 144418
[16] McKee R A, Walker F J and Chisholm M F 1998 *Phys. Rev. Lett.* **81** 3014
[17] Hong X, Posadas A and Ahn C H 2005 *Appl. Phys. Lett.* **86** 142501
[18] Vogt T, Hriljac J A, Hyatt N C and Woodward P 2003 *Phys. Rev. B* **67** 140401
[19] Biskup N, Salafranca J, Mwhta V, Oxley M P, Suzuki Y, Pennycook S J, Pantelides S T and Varela M 2014 *Phys. Rev. Lett.* **112** 087202
[20] Bai Y H, Wang X, Mu L P and Xu X H 2016 *Chin. Phys. Lett.* **33** 087501
[21] Seo H, Posadas A B, Mitra C, Kvit A V, Ramdani J and Demkov A A 2012 *Phys. Rev. B* **86** 075301
[22] Sterbinsky G E, Nanguneri R, Ma J X, Shi J, Karapetrova E, Woicik J C, Park H, Kim J W and Ryan P J 2018 *Phys. Rev. Lett.* **120** 197201
[23] Feng Q Y, Meng D C, Zhou H B, Liang G H, Cui Z Z, Huang H L, Wang J L, Guo J H, Ma C, Zhai X F, Lu Q Y and Lu Y L 2019 *Phys. Rev. Mater.* **3** 074406
[24] Aschauer U, Pfenninger R, Selbach S M, Grande T and Spaldin N A 2013 *Phys. Rev. B* **88** 054111
[25] Golosova N O, Kozlenko D P, Kolesnikov A I, Yu V Kazimirov, Smirnov M B, Jirak Z and Savenko B N 2007 *Phys. Rev. B* **83** 214305
[26] Lan Q Q, Zhang X J, Shen X, Zhang J, Guan X X, Yao Y, Wang Y G, Yu R C, Peng Y and Sun J R 2015 *Appl. Phys. Lett.* **107** 242404
[27] Yokoyama Y, Yamasaki Y, Taguchi M, Hirata Y, Takubo K, Miyawaki J, Harada Y, Asakura D, Fujioka J, Nakamura M, Daimon H, Kawasaki M, Tokura Y and Wadati H 2018 *Phys. Rev. Lett.* **120** 206402
[28] Cabero M, Nagy K, Gallego F, Sander A, Rio M, Cuellar F A, Tornos J, Hernandez-Martin D, Nemes N M, Mompean F, Garcia-Hernandez M, Rivera-Calzada A, Sefrioui Z, Reyren N, Feher T, Varela M, Leon C and Santamaria J 2017 *APL Mater.* **5** 096104
[29] Zhang N B, Zhu Y L, Li D, Pan D S, Tang Y L, Han M J, Ma J Y, Wu B, Zhang Z D and Ma X L 2018 *Appl. Mater. Interfaces* **10** 38230
[30] Wei W G, Wang H, Zhang K, Liu H, Kou Y F, Chen J J, Du K, Zhu Y Y, Hou D L, Wu R Q, Yin L F and Shen J 2015 *Chin. Phys. Lett.* **32** 087504
[31] An Q C, Xu Z, Wang Z Z, Meng M, Guan M X, Meng S, Zhu X T, Guo H Z, Yang F and Guo J D 2021 *Appl. Phys. Lett.* **118** 081602
[32] Huang H L, Zhang J N, Zhang H, Han F R, Chen X B, Song J H, Zhang J, Qi S J, Chen Y S, Cai J W, Hu F X, Shen B G and Sun J R 2020 *J. Phys. D* **53** 155003
[33] Li S S, Wang J S, Zhang Q H, Roldan M A, Shan L, Jin Q, Chen S, Wu Z P, Wang C, Ge C, He M, Guo H Z, Gu L, Jin K J and Guo E J 2019 *Phys. Rev. Mater.* **3** 114409
[34] Meng D C, Guo H L, Cui Z Z, Ma C, Zhao J, Lug J B, Xu H, Wang Z C, Hu X, Fu Z P, Peng R R, Guo J H, Zhai X F, Browni G J, Knizej R and Lu Y L 2018 *Proc. Natl. Acad. Sci. USA* **115** 2873
[35] Lu Q Y and Yildiz B 2015 *Nano Lett.* **16** 1186
[36] Lei H T, Zhang Q X, Wang Y B, Gao Y M, Wang Y Z, Liang Z Z, Zhang W and Cao R 2021 *Dalton Trans.* **50** 5120
[37] Jeen H, Choi W S, Freeland J W, Ohta H, Jung C U and Lee H N 2013 *Adv. Mater.* **25** 3651
[38] Li J, Guan M X, Nan P F, Wang J, Ge B H, Qiao K M, Zhang H R, Liang W H, Hao J Z, Zhou H B, Shen F R, Liang F X, Zhang C, Liu M, Meng S, Zhu T, Hu F X, Wu T, Guo J D, Sun J R and Shen B G 2020 *Nano Energy* **78** 105215
[39] Liu H F, Shi L, Guo Y Q, Zhou S M, Zhao J Y, Wang C L, He L F and Li Y 2014 *J. Alloys Compd.* **594** 158
[40] Miao X B, Wu L, Lin Y, Yuan X Y, Zhao J Y, Yan W S, Zhou S M and Shi L 2019 *Chem. Commun.* **55** 1442